



Earthquake-generated tsunamis in the Mediterranean Sea: Scenarios of potential threats to Southern Italy

Stefano Lorito,¹ Mara Monica Tiberti,¹ Roberto Basili,¹ Alessio Piatanesi,¹ and Gianluca Valensise¹

Received 19 January 2007; revised 24 August 2007; accepted 21 September 2007; published 9 January 2008.

[1] We calculated the impact on Southern Italy of a large set of tsunamis resulting from earthquakes generated by major fault zones of the Mediterranean Sea. Our approach merges updated knowledge on the regional tectonic setting and scenario-like calculations of expected tsunami impact. We selected three potential source zones located at short, intermediate and large distance from our target coastlines: the Southern Tyrrhenian thrust belt; the Tell-Atlas thrust belt; and the western Hellenic Arc. For each zone we determined a Maximum Credible Earthquake and described the geometry, kinematics and size of its associated Typical Fault. We then let the Typical Fault float along strike of its parent source zone and simulated all tsunamis it could trigger. Simulations are based on the solution of the nonlinear shallow water equations through a finite difference technique. For each run we calculated the wavefields at desired simulation times and the maximum water elevation field, then produced traveltime maps and maximum wave-height profiles along the target coastlines. The results show a highly variable impact for tsunamis generated by the different source zones. For example, a large Hellenic Arc earthquake will produce a much higher tsunami wave (up to 5 m) than those of the other two source zones (up to 1.5 m). This implies that tsunami scenarios for Mediterranean Sea countries must necessarily be computed at the scale of the entire basin. Our work represents a pilot study for constructing a basin-wide tsunami scenario database to be used for tsunami hazard assessment and early warning.

Citation: Lorito, S., M. M. Tiberti, R. Basili, A. Piatanesi, and G. Valensise (2008), Earthquake-generated tsunamis in the Mediterranean Sea: Scenarios of potential threats to Southern Italy, *J. Geophys. Res.*, 113, B01301, doi:10.1029/2007JB004943.

1. Introduction

[2] Tsunamis in the Mediterranean Sea have often caused severe damage and loss of lives. Although they are less frequent than those of the Pacific or Indian oceans, some of them are well known from historical accounts, such as those following the $M > 8$, 365 AD and 1303 earthquakes near Crete and the $M > 7$, 1222 earthquake near Cyprus. Also, a devastating tsunami hit the coasts of Sicily and Calabria in 1908 following a $M > 7$ earthquake in the Messina Straits. Nonetheless, and despite the existence of European tsunami catalogues for the Mediterranean region [Soloviev, 1990; Tinti *et al.*, 2001; Tinti *et al.*, 2004], it was not until the devastating 2004 tsunami in the Indian Ocean that more systematic studies have been undertaken in the Euro-Mediterranean area (e.g., project TRANSFER, EC 6th Framework Programme: <http://www.transferproject.eu/>), and in Italy (e.g., Italy's Department for Civil Defense projects, <http://www.ingv.it/progettiSV/>).

[3] The purpose of this work is to start up a thorough investigation of earthquake-related tsunamis in the Mediterranean area and a systematic assessment of the associated hazards. We begin by focusing on the expected tsunami impact on the coasts of Southern Italy, but our method can be easily extended to the entire Mediterranean basin. Although other source types, such as large submarine landslides [e.g., Pareschi *et al.*, 2006a] or volcanic activity [e.g., Tinti *et al.*, 2006; Pareschi *et al.*, 2006b] have been invoked to explain large historical and pre-historical tsunamis in the Mediterranean, we focused on strictly earthquake-generated tsunamis because their impact can be systematically addressed based on existing knowledge. We thus identify the main tsunamigenic structures in the Mediterranean area (Figure 1) by combining geological and tectonic data with historical and instrumental records. We benefit from the expertise developed in the preparation of the Database of Individual Seismogenic Sources [DISS: Valensise and Pantosti, 2001], and particularly of its most recent version (<http://www.ingv.it/DISS/>; see also R. Basili *et al.*, The Database of Individual Seismogenic Sources (DISS), version 3: Summarizing 20 years of research on Italy's earthquake geology, submitted to *Tectonophysics*, 2007), to extend the mapping of seismogenic and potentially tsunamigenic sources to the whole central Mediterranean

¹Istituto Nazionale di Geofisica e Vulcanologia, Sezione di Sismologia e Tettonofisica, Rome, Italy.

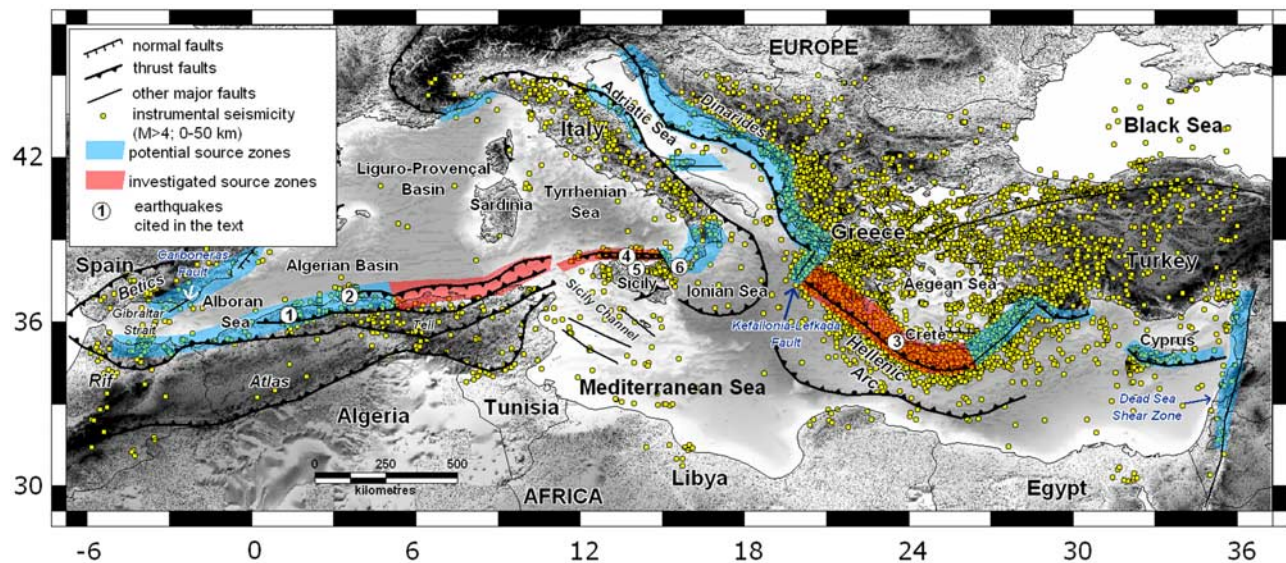


Figure 1. Tectonic sketch map of the Mediterranean basin. Instrumental seismicity (yellow dots; $M > 4$; depth 0–50 km) is taken from the ISC Catalogue (ISC, 2004). Color-shaded ribbons highlight the main structures capable of generating tsunamis that pose significant hazard to Mediterranean shore-facing settlements (shown in blue or red. Those shown in red have been investigated in this work). Selected earthquakes are shown with circles: 1) El Asnam, 1980; 2) Boumerdes, 2003; 3) Crete, 365 AD; 4) Palermo, 2002; 5) Northern Sicily, 1823; 6) Messina Straits, 1908.

area. Our approach allows preliminary tsunami scenarios to be supplied to their potential end-users while they are being progressively updated at the same pace as the advances in source mapping.

[4] So far most simulations of earthquake-induced tsunamis in the Mediterranean have focused on the reconstruction of specific past events [e.g., *Tinti and Piatanesi, 1996; Piatanesi and Tinti, 1998; El-Sayed et al., 2000; Piatanesi and Tinti, 2002; Alasset et al., 2006; Gutscher et al., 2006; Hamouda, 2006*] with the main purpose of constraining the earthquake source parameters. Others have used hypothetical or inferred earthquake source parameters for constructing tsunami scenarios [e.g., *Pelinovsky et al., 2002; Tinti et al., 2005*]. Tsunami simulations oriented to both tsunami hazard estimation and forecasting, involving parameterization of extended sources, exist also for other zones of the world such as North-East Pacific [*Titov et al., 2005; Geist and Parsons, 2006*], Japan [*Satake et al., 1996; Yamazaki et al., 2006*], Thailand [*Løvholt et al., 2006*], and New Zealand [*Berryman, 2005; Power et al., 2007*].

[5] In this pilot study we focused on three major extended tsunamigenic structures, hereinafter referred to as Source Zones (SZs): the southern Tyrrhenian Sea thrust system, the Tell system in the Algeria-Tunisia offshore and the Hellenic Arc, respectively located at short, intermediate and large distance from the coasts of Southern Italy (Figure 1). For each of these potential source zones we first defined the geometrical parameters of seismogenic faults based on geological and seismological evidence and assessed the size of the expected earthquakes. We then computed several tsunami scenarios by letting the position of the fault shift at regular steps along each of the three SZs. Each individual scenario yields the wavefields at specified times and locations throughout the Mediterranean basin and the maximum

water elevation field, that supplies at-glance information on the tsunami energy distribution during its whole propagation. We then analyzed each scenario and extracted (a) the maximum wave heights expected along the Southern Italy coasts for each single scenario; (b) the average and standard deviation estimates of the maximum wave height due to the set of scenarios pertaining to each SZ; and (c) the tsunami traveltime maps for the investigated tsunamigenic source zones.

2. Method

[6] This section illustrates the reasoning we adopted for constructing tsunami scenarios.

[7] A Source Zone includes an active tectonic structure at regional scale. The geometric and kinematic properties of the structure are assumed to exhibit only limited variations inside the SZ; similarly, the rheological and dynamic properties of the tectonic structure are assumed to allow equally large earthquakes to be released all throughout the SZ.

[8] We then assumed a SZ is made up of a number of individual fault segments, each of them capable of releasing an earthquake. For each SZ we identified a Maximum Credible Earthquake (MCE) and an associated Typical Fault (TF). We let the TF float along the entire SZ and computed a tsunami scenario at regular intervals. This procedure allows a number of potential scenarios to be explored based on the information that is more robust (the location and geometry of the fault(s)) without having to worry about the exact location of the ends of the coseismic rupture. In other words, the limited knowledge on the internal structure of the SZ, and hence of any permanent segment boundaries, is coped with simply by ignoring the possibility that such boundaries exist.

Table 1. Summary of Parameters of the TFs Shown in Figures 3, 4, and 5^a

	L, km	W, km	D, km	Slip, m	Strike, deg	Dip, deg	Rake, deg	MCE, M_w
Algeria-Tunisia	35	13.5	1	4	72	30	90	7.1
Southern Tyrrhenian	12	7	3	1	273	45	90	6.2
Hellenic Arc	130	86	5	17.5	314	35	90	8.4

^aL: Length; W: Down-dip width; D: Depth of top edge of fault below sea level.

[9] The full procedure is summarized below in schematic pseudo-code form. Detailed descriptions of each step follow.

define SOURCE ZONES

choose COASTLINES

for each SOURCE ZONE

define MAX CREDIBLE EARTHQUAKE and TYPICAL FAULT (M_w , rake, dip, length, width, depth, slip)

define SIMULATION PARAMETERS (domain size, spatial resolution, time step)

place VIRTUAL TIDE-GAUGES

for each TYPICAL FAULT

move TYPICAL FAULT *along the* SOURCE ZONE *at* L *or* L/2 *steps*

and define discrete TSUNAMIGENIC SOURCES (lat, lon, strike)

calculate HMAXs, TRAVEL TIMES, MARIGRAMS *at* VIRTUAL TIDE-GAUGES

End

for each COASTLINE

Calculate MAXIMUM *of* HMAXs, AVERAGE *of* HMAXs, STANDARD DEVIATION *of* HMAXs

End

End

[10] To assess the MCE for each SZ we selected the largest earthquake that has ever occurred in that zone and for which there exists, or is possible to obtain, a reliable magnitude estimation. We therefore took into account historical and instrumental catalogues, such as the CFTI catalogue [Boschi *et al.*, 2000], the CPTI04 catalogue [Gruppo di lavoro CPTI, 2004], the ISC On-line Bulletin (<http://www.isc.ac.uk/>), the Global CMT catalogue (<http://www.globalcmt.org/>), the EMMA database [Vannucci and Gasperini, 2004] (and its up-to-date electronic version at <http://ibogfs.df.unibo/user2/paolo/www/EMMA30/>), and recent literature on the seismotectonics of the study regions. We assumed that such an earthquake may repeat anywhere within its parent SZ at any time in the future, and used its moment magnitude to constrain the size of the TF.

[11] The TF is defined by parameters that must comply with both the seismological properties of the MCE and the tectonic properties of its parent SZ. To estimate them we made extensive use of data available in the literature and particularly in the DISS database (<http://www.ingv.it/DISS/>). Geologic maps and cross sections, seismic reflection profiles, geodetic data, seismic tomography, and coastal uplift data were used to constrain the geometry of the fault. Where we lacked data we constrained fault size using the empirical relationships by Wells and Coppersmith [1994]. For strike, dip and rake we used all available information from geological maps based on surface and subsurface data and from focal mechanisms (CMT, EMMA). Further constraints on rake were obtained from maps of the principal

stress and strain axes and from GPS velocity fields. The fault top and bottom depth was estimated through geological sections, seismic tomography images, depth distributions of instrumental earthquakes. The amount of slip for a single rupture event was derived from the seismic moment of the MCE. Dealing exclusively with contractional structures, we also verified that fault area and fault slip were consistent with a fault model having average static stress drop between 80 and 150 bar, that are commonly observed values for reverse faulting mechanisms, using the formulations by Kanamori and Brodsky [2004].

[12] The TF was let floating at regular steps along the strike of the SZ. At each new position of the TF, strike, dip and rake were slightly adjusted to account for the internal geometric variations of the SZ. Steps were taken at one fault length. In the case of the Hellenic Arc SZ, shifting was taken at half fault length (65 km, see Table 1) to guarantee a sufficient spatial sampling of the tsunamigenic structure. At each new position the TF was made to release its MCE by uniform slip over the entire fault plane. Rupture was assumed to be instantaneous, because the typical timescale of a tsunami is usually much larger than the rupture timescale.

[13] In established simulation practice, tsunami waves are considered as long shallow-water gravity waves because their wavelength is usually much larger than sea depth. In this study we used the nonlinear shallow water equations written as follows:

$$\begin{aligned} \frac{\partial(z+h)}{\partial t} + \nabla \cdot [\mathbf{v}(z+h)] &= 0 \\ \frac{\partial \mathbf{v}}{\partial t} + (\mathbf{v} \cdot \nabla) \mathbf{v} &= -g \nabla z + \mathbf{C} + \mathbf{F} \end{aligned} \quad (1)$$

where z is the water elevation above sea level, h is the water depth in a still ocean, \mathbf{v} is the depth-averaged horizontal velocity vector, g is the gravity acceleration, \mathbf{C} is the Coriolis force, and F represents bottom friction forces, for which we used the Manning's formula with a roughness coefficient of 0.05. The equations were solved numerically by means of a finite difference method on a staggered grid [Mader, 2001]. We set the boundary conditions as pure wave reflection at the solid boundary, by setting to zero the velocity component perpendicular to the coastline. In this way all tsunami kinetic energy is converted into potential energy at the coast. This is equivalent to the physical condition achieved when the wave reaches the maximum onshore inundation distance. Thus while we do not simulate the complex processes of inundation (which are controlled by fine scale details of the nearshore topography), our predicted coastal wave heights include wave shoaling in shallow waters and could be a rough proxy for the inundation effects. Full wave transmission $\mathbf{v} \cdot \mathbf{n} = (g/c)z$ is set at

Table 2. Summary of Basic Parameters for the Tsunami Simulation in Each SZ

SZ	Spatial Resolution, arc-min	Time Step, sec	Floating Step, km	Number of Simulations
Algeria-Tunisia	0.5	1.5	L = 35	15
Southern Tyrrhenian	0.25	0.5	L = 12	27 South dipping 26 North dipping
Hellenic Arc	1	2.5	L/2 = 65	9

the open boundary (open sea), where $c = \sqrt{gh}$ is the wave phase velocity and \mathbf{n} is the unit vector normal to the boundary and directed outwardly. The initial seawater elevation was assumed to be equal to the coseismic vertical displacement of the sea bottom produced by the TF, computed through the *Okada* [1985, 1992] analytical formulation. The initial velocity field was assumed to be identically zero. The seafloor topography was taken from the ETOPO2 bathymetric data set [Smith and Sandwell, 1997].

[14] To achieve a detailed sampling of the source field we set a different spatial resolution for each SZ; time steps were adjusted accordingly to guarantee numerical stability (see Table 2). A significant trade-off exists between CPU time and the need to extend the calculations to a large enough area to include significantly high tsunami waves. To find an optimal balance between these contrasting needs we used a different computational domain for each SZ.

[15] We performed a distinct numerical experiment for each fault position in each SZ for a total of 77 runs. During each simulation we calculated and stored for subsequent analyses the following quantities:

[16] 1) the absolute maximum values of water height (HMAX) reached during tsunami propagation at each node of the computational domain;

[17] 2) the traveltimes of tsunami waves, calculated by picking first arrivals of waves with positive amplitude (wave crests) at each grid node;

[18] 3) the time evolution of water height (marigram) at some coastal localities.

[19] To calculate marigrams, we selected a set of principal harbors and densely populated coastal sites as virtual tide-gauge stations. Figure 2 shows their location along the coasts of Southern Italy. From each simulation and for each of the three target areas (coastlines of Sicily, Sardinia and peninsular Southern Italy; Figure 2) we extracted three HMAX profiles. For each point along these coastlines the HMAX values produced by each single potential source were grouped according to the source zone. Finally, we calculated the absolute maximum, the average, and the standard deviation of all coastal HMAX values for each source zone.

3. Selected Tsunamigenic Source Zones

[20] The Mediterranean Sea has a very complex tectonic setting resulting from the fragmentation of the plate boundary between Africa and Eurasia into distinct subduction zones, each one characterized by a diverse subduction style (e.g., *Faccenna et al.* [2004], and references therein; Figure 1). The geometry of tectonic structures may change

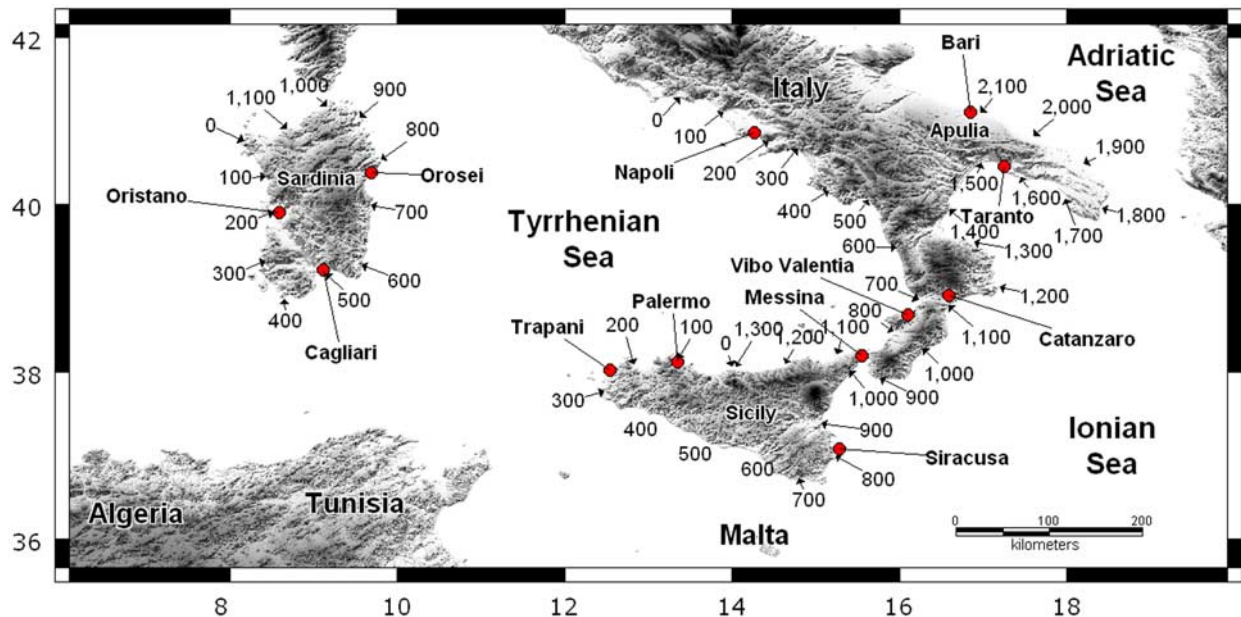


Figure 2. Map showing distance (km) along target coastlines where the tsunami impact was estimated. Selected locations of virtual tide-gauge stations are also shown (red dots). This map is intended for use in conjunction with Figures 3, 4, 5, 6, 7 and 8.

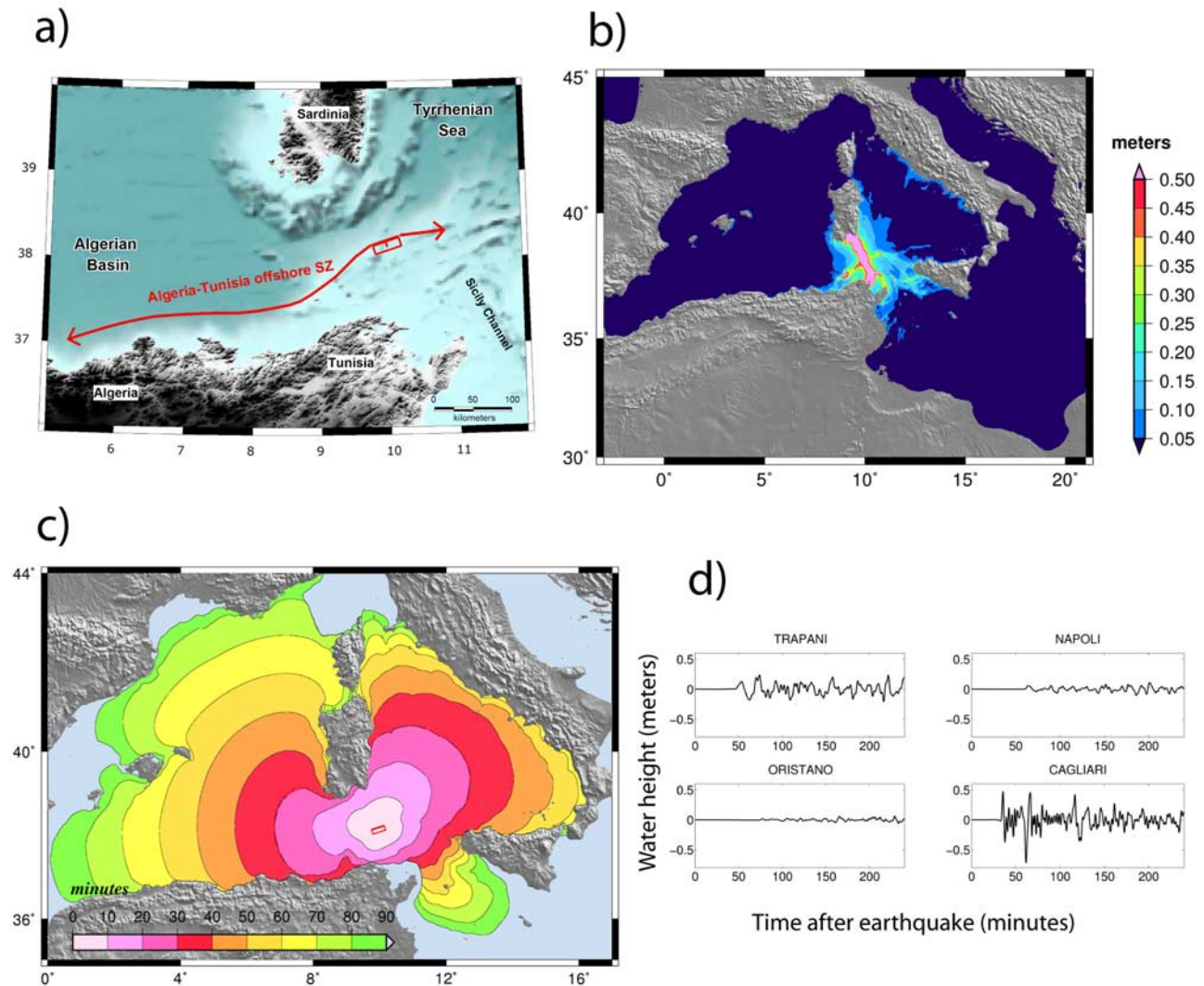


Figure 3. Algeria-Tunisia offshore Source Zone. a) Map of the source zone. The double-headed arrow indicates the floating path of the Typical Fault (see Table 1 for its parameters). b) Map of the maximum wave height in the simulation domain for the tsunami generated by the selected TF. c) Traveltime map of the tsunami frontal crest generated by the TF (red rectangle); contours are plotted at 10 min intervals. d) Marigrams at selected virtual tide gauges for the tsunamis generated by the TF (time in minutes after the earthquake, water height in meters).

abruptly from place to place, and deformation rates change accordingly. Major earthquakes occur systematically along known fault zones. The largest magnitude earthquakes are associated with convergent boundaries, such as the Hellenic Arc, the Dinarides thrust front, the North African Rif and Tell systems, and with a few major strike-slip structures, such as the Dead Sea Shear Zone, the Kefallonia-Lefkada Fault (western Greece), and the Carboneras Fault (southern Spain). Most of these boundaries run close to the coastlines or in the open sea, and are thus potential sources for large tsunamis.

[21] This section describes the local tectonic setting of three selected Source Zones along with the criteria we followed to define the Typical Fault (TF) used in the modeling.

3.1. Algeria-Tunisia Offshore Source Zone

[22] The Algeria-Tunisia offshore zone (Figure 3a) is part of a 1,500 km-long and up to 150 km-wide contraction belt,

running roughly E-W from the Gibraltar Strait to the Sicily Channel. This zone is widely known as the Tell-Atlas thrust system, which accommodates a significant portion of the Africa-Europe convergence in the western Mediterranean. The NW-SE Africa-Europe convergence takes place at ~ 5 mm/y [e.g., *Nocquet and Calais, 2004; Serpelloni et al., 2007*], whereas the shortening rate across the thrust belt is estimated at ~ 2 mm/y [*Meghraoui and Doumaz, 1996*]. These figures indicate that the onshore part of the thrust system accommodates only about 40% of the total deformation. Thus an important part of the convergence must be accommodated elsewhere, e.g., offshore in the Alboran-Algerian basin or in the Betic region [e.g., *Domzig et al., 2006*].

[23] Although the seismicity along the contraction belt is rather sparse, available focal mechanisms indicate a clear NNW-SSE maximum horizontal stress axis. Reverse fault-

ing dominates along most of the Tell-Atlas, whereas strike-slip earthquakes are more frequent at the very western end of the belt [see *Vannucci et al.*, 2004; *Serpelloni et al.*, 2007].

[24] The largest known earthquake of Tell-Atlas belt took place near El Asnam (Algeria) on 10 October 1980. This M_w 7.1 earthquake (Global CMT catalog) was generated by a north-dipping, E-W striking thrust [*Ruegg et al.*, 1982; *Philip and Meghraoui*, 1983; *Bezzeghoud et al.*, 1995]. In 2003, a smaller (M_w 6.8) but much more catastrophic thrust faulting earthquake occurred off the Algerian coast, in front of the densely inhabited city of Boumerdes. This earthquake supplied living evidence for the existence of a previously unknown tectonic trend and therefore has strong implications for the assessment of seismic hazard in the region [*Déverchère et al.*, 2005].

[25] Most of the models proposed for the 2003 earthquake invoke a south-dipping causative fault [*Delouis and Vallée*, 2003; *EERI Reconnaissance Report*, 2003; *Delouis et al.*, 2004; *Meghraoui et al.*, 2004; *Semmane et al.*, 2005], whereas all mapped active faults onshore are north-dipping thrusts. If the south-dipping solution is reliable, the Boumerdes fault might be part of an offshore system formed by a set of Plio-Quaternary structures running parallel to the already known Tell system. This portion of the thrust system was first detected by *Déverchère et al.* [2003], who related tectonic features identified from bathymetric data with the surface expression of the 2003 earthquake rupture, and then analyzed more extensively by *Yelles et al.* [2004], *Déverchère et al.* [2005], *Domzig et al.* [2006]. This offshore system may thus accommodate part of the convergence between Europe and Africa and be capable of earthquakes up to magnitude ~ 7.0 . *Déverchère et al.* [2005] and *Domzig et al.* [2006] also suggested that this system is the result of an incipient stage of subduction of the oceanic crust of the Algerian basin beneath Africa. The tsunami that affected the Algerian and Spanish coasts after the 2003 Boumerdes earthquake [*Hébert and Alasset*, 2003; *Alasset et al.*, 2006] supplied living evidence of the tsunamigenic potential of this area.

[26] The good lateral continuity of the Tell thrust system suggests that this structure is capable of generating earthquakes on both north- and south-dipping faults. Main faulting in the offshore part of the system seems to occur on south-dipping planes. We set the western end of the Algeria-Tunisia SZ arbitrarily, i.e., not coincident with any known structural element. We then adopted the 1980 El Asnam earthquake as the MCE even though it occurred on a north-dipping plane beyond the western end of the SZ (Figure 1). We sized the TF after the moment magnitude of this earthquake as taken from the Global CMT catalog. Strike and dip of the TF were defined on the basis of published tectonic maps of the south-dipping faults in key areas and extended along the trace of the entire SZ.

3.2. Southern Tyrrhenian Source Zone

[27] An E-W narrow contraction belt runs from the Sicily Channel to the Aeolian Islands, about 50 km off the northern Sicily coast (Figure 4a). This region is thought to accommodate 4–5 mm/y of the Africa-Europe convergence [*D'Agostino and Selvaggi*, 2004; *Serpelloni et al.*, 2005]

that takes place at ~ 5 –8 mm/y [*Goes et al.*, 2004; *Pondrelli et al.*, 2004, and references therein; *Serpelloni et al.*, 2007].

[28] In the past 30 a frequent events with $M > 5$ originated in this area, including the 6 September 2002, M_w 5.9, Palermo earthquake [*Goes et al.*, 2004; *Pondrelli et al.*, 2004; *Vannucci et al.*, 2004]. They are mostly shallow earthquakes having compressional focal mechanisms with a P-axis oriented NNW-SSE. This trend of contraction is well consistent with plate motion vectors from GPS data [see *D'Agostino and Selvaggi*, 2004; *Pondrelli et al.*, 2004; *Vannucci et al.*, 2004 and references therein]. Some moderate-size historical earthquakes are likely to belong to this seismic belt [e.g., *Jenny et al.*, 2006], at least one of which (5 March 1823, M_w 5.9) generated a tsunami [*Boschi et al.*, 2000; *Tinti et al.*, 2004].

[29] The available data are not sufficient to constrain the dip direction of the major faults based on focal mechanisms, but the north-dipping planes are often preferred because they are consistent with known pre-existing structures. In particular, the so-called Drepano thrust front, interpreted as a Miocene suture between the Kabilo-Calabride domain (southern margin of the European plate) and the Sicily-Maghrebian chain (Africa northern margin), is thought to be the source of the 2002, Palermo earthquake [*Pepe et al.*, 2005]. The tectonic architecture of this area, however, is quite similar to that of the Algerian offshore, where part of the Africa-Europe convergence is consumed by active south-dipping structures developed at the boundary between the Tell chain and the oceanic crust of the Algero-Provençal Basin [*D'Agostino and Selvaggi*, 2004; *Déverchère et al.*, 2005]. As recent interpretations [*D'Agostino and Selvaggi*, 2004; *Goes et al.*, 2004] hypothesized active south-dipping thrusting in the Southern Tyrrhenian Sea in recent times (0.8–0.5 Ma), we considered the south-dipping plane more reliable. For the purpose of our computations we therefore used two hypothetical faults having opposite dip direction.

[30] The MCE for this SZ was based on the 5 March 1823 earthquake, the largest event reported in current catalogues [*Boschi et al.*, 2000; *Gruppo di lavoro CPTI*, 2004]. This event is located on the northern coast of Sicily, but, due to inherent difficulties in locating earthquakes in coastal areas and to the shape of its damage pattern, we assumed it belongs to the offshore seismic belt and adopted as reference earthquake. Its reported magnitude based on a large set of macroseismic data is M_w 5.9, but we believe this value is underestimated as a result of its offshore location. We therefore arbitrarily increased it by 0.3 units up to M_w 6.2, still below the maximum potential of $M \geq 7.0$ estimated for this tectonic region by *Jenny et al.* [2006] or *Billi et al.* [2007].

3.3. Hellenic Arc Source Zone

[31] The subduction of the African plate beneath the Aegean (Figure 5a) extends from the Kefallonia-Lefkada lineament to the west, to the eastern end of the island of Rhodes to the east [*Papazachos and Nolet*, 1997; *Papazachos et al.*, 2000; *Wortel and Spakman*, 2000; *Faccenna et al.*, 2003; *Piromallo and Morelli*, 2003]. Here the NNE-SSW convergence between Africa and the Aegean is thought to take place at ~ 4 –5 cm/y [e.g., *Papazachos and Papazachou*, 1997 and references therein], and GPS velocities are the fastest

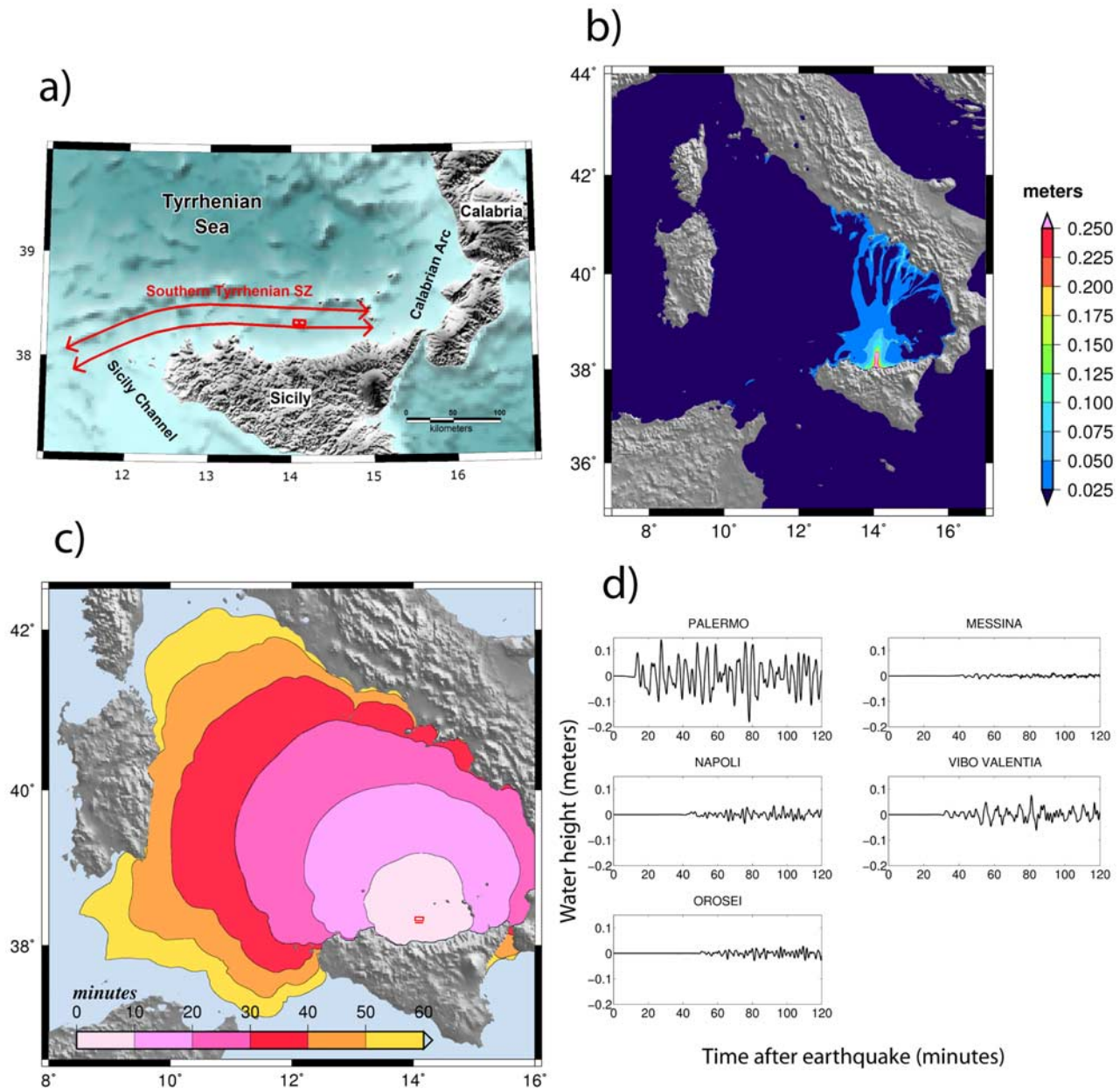


Figure 4. Southern Tyrrhenian Source Zone. See Figure 3 for panel and symbol explanations.

detected in the entire Mediterranean basin [Kahle *et al.*, 2000; McClusky *et al.*, 2000].

[32] The Hellenic Arc has historically proven to be capable of frequent and occasionally very large earthquakes ($M > 8$) related to the subduction of the Ionian oceanic crust under the Aegean; in fact, this is the most active region in the entire Mediterranean [Vannucci *et al.*, 2004]. One of the most impressive earthquakes of ancient times hit western Crete in 365 AD, generating a tsunami that affected the coasts of the entire eastern and central Mediterranean [Guidoboni *et al.*, 1994; Papazachos and Papazachou, 1997]. Subduction-related shallow seismicity concentrates along the Hellenic trench system. Further north, the depth of the earthquakes progressively deepens down to 200 km, outlining a gently dipping ($\sim 30^\circ$) Benioff zone. The focal mechanisms of earthquakes shallower than 40 km consis-

tently show NE-SW compression coherent with plate motion vectors [Papazachos *et al.*, 2000; Benetatos *et al.*, 2004; Vannucci *et al.*, 2004; Bohnhoff *et al.*, 2005].

[33] The eastern and western parts of the Hellenic subduction zone exhibit a quite different behavior. East of Crete, focal mechanisms become heterogeneous, including strike-slip solutions as the plate boundary becomes parallel to the vectors of relative plate motion [Benetatos *et al.*, 2004; Vannucci *et al.*, 2004]. It is also worth noting that from the Kefallonia-Lefkada islands to the eastern end of Crete the subducting oceanic crust is in contact with the continental crust of the overriding plate, whereas to the east of Crete the two crusts are decoupled [Makris and Yegorova, 2006].

[34] We considered the 365 AD earthquake as the MCE for this area. The characteristics of its source are based on a

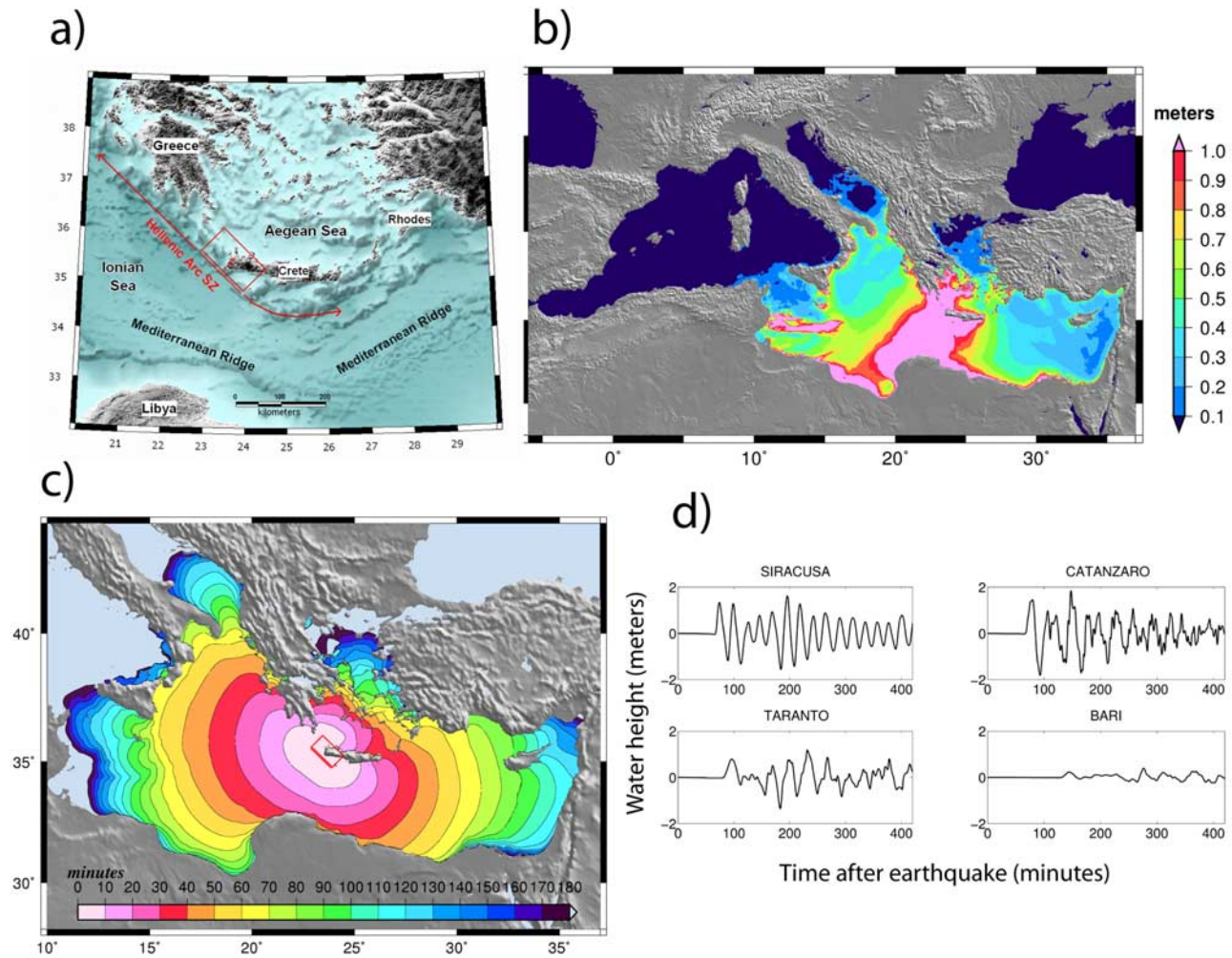


Figure 5. Hellenic Arc Source Zone. See Figure 3 for panel and symbol explanations.

good set of data on raised shorelines (up to 9 m in SW Crete) that have long been interpreted as the effect of coseismic uplift [Flemming, 1978; Pirazzoli *et al.*, 1982, 1996; Stiros and Drakos, 2006]. We estimated the earthquake magnitude as M_w 8.4 by modeling the fault dislocation [Okada, 1985] to fit the vertical displacement field given by this coastal uplift data set.

[35] Strike and dip are taken parallel to the orientation of the subduction plane (extensively investigated through gravity, seismic and tomographic techniques; e.g., Papazachos and Nolet [1997]; Bohnhoff *et al.* [2001]; Casten and Snopek [2006]; Makris and Yegorova [2006]) and based on focal mechanisms. The rake is taken parallel to the plate motion vectors derived from GPS data and focal mechanisms. Finally, as the Hellenic subduction zone cannot be considered a single tectonic structure, we assumed that the lithospheric volume capable of 365 AD-like earthquakes should coincide with the zone where the two plates are coupled and focal mechanisms are homogeneous, and should be located between 5 and 60 km depth.

4. Results

[36] This section illustrates the results obtained for all simulations in each SZ. The HMAX maps (Figures 3b, 4b

and 5b), the tsunami traveltimes maps (Figures 3c, 4c and 5c) and the marigram plots (Figures 3d, 4d and 5d) are all related to a single sample TF for each SZ. Conversely, the total number of simulations we performed yielded 77 HMAX maps and 77 traveltime maps. For each of the 77 simulations we calculated marigrams at each of the virtual tide gauges along the coasts of Italy. Conversely, Figures 6, 7, and 8 show the tsunami impact along the coastlines of Sicily, peninsular Southern Italy and Sardinia, respectively, for all the simulations performed for each SZ. The impact of the tsunami wave is shown as a profile of the aggregated HMAXs maximum, average and average plus one standard deviation, at each point of all selected coastline stretches. Distances along the coastlines (in km) are taken from an arbitrary starting point and increase counter-clockwise (Figure 2). They are not intended to be accurate distance measurements but rather to be a practical way to identify positions along the coastlines.

4.1. Algeria-Tunisia Offshore Source Zone

[37] Figure 3b shows the HMAX values reached during propagation of a tsunami generated by the TF releasing the MCE of this Source Zone (Figure 3a) Most of the tsunami energy (roughly corresponding with the area where the wave height exceeds 0.5 m) focuses mainly into two

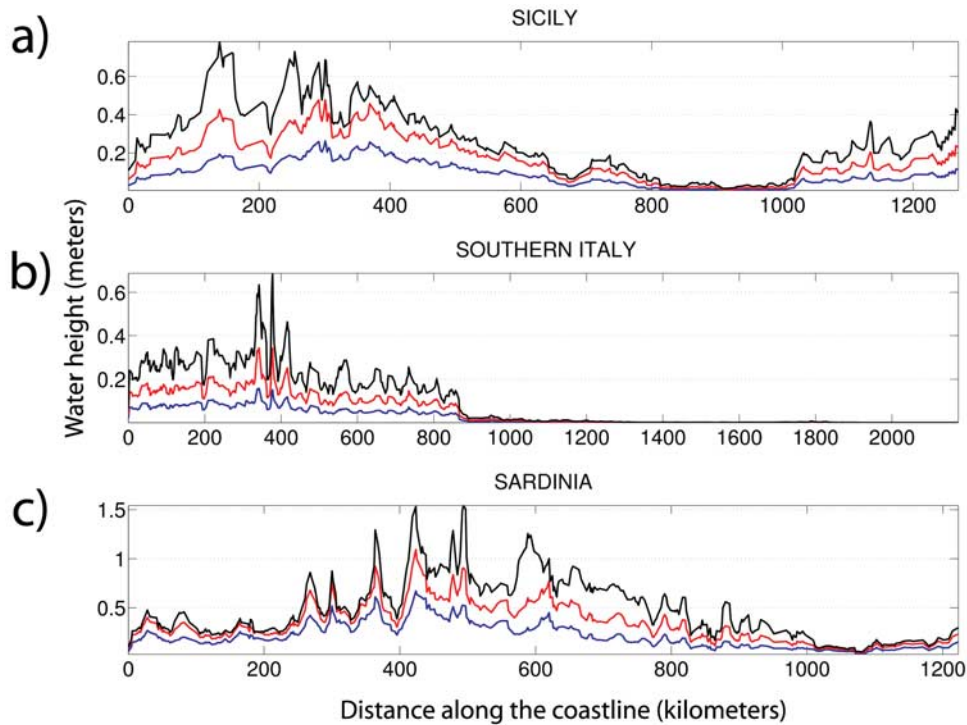


Figure 6. Algeria-Tunisia offshore Source Zone. Diagram of tsunami impact along the coastlines of a) Sicily, b) peninsular Southern Italy, and c) Sardinia, shown as aggregated HMAX maximum (black), average (blue) and average plus one standard deviation (red) of the wave generated by all the faults let floating along the SZ. Horizontal scales are distances in kilometers: see Figure 2 for locating the diagram relative to the coastline. Vertical scales are water heights in meters.

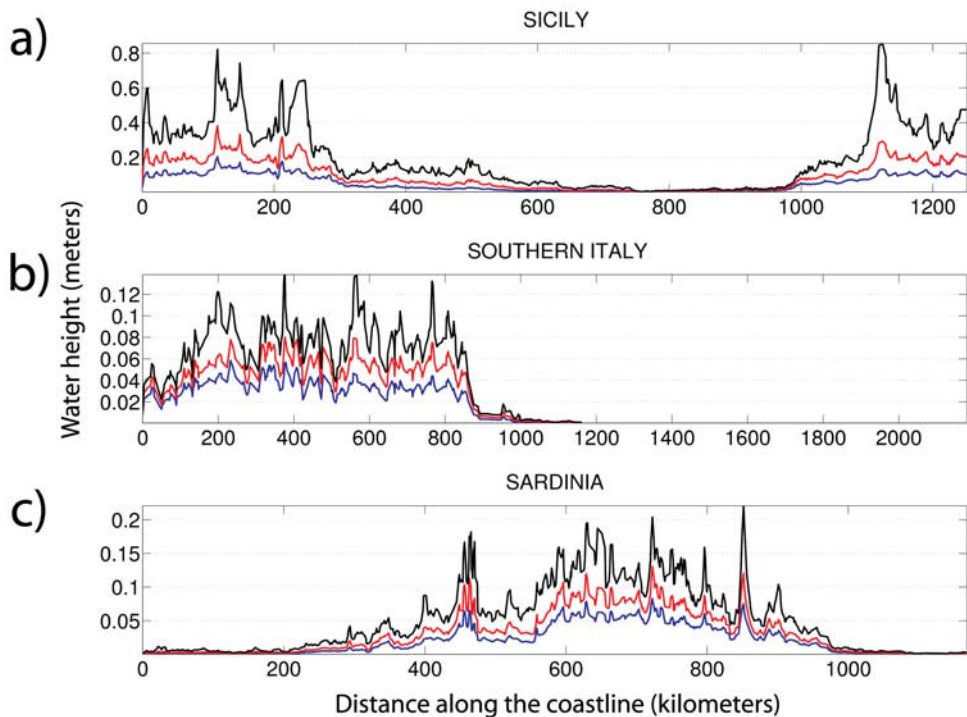


Figure 7. Southern Tyrrhenian Source Zone. See Figure 6 for panel and symbol explanations.

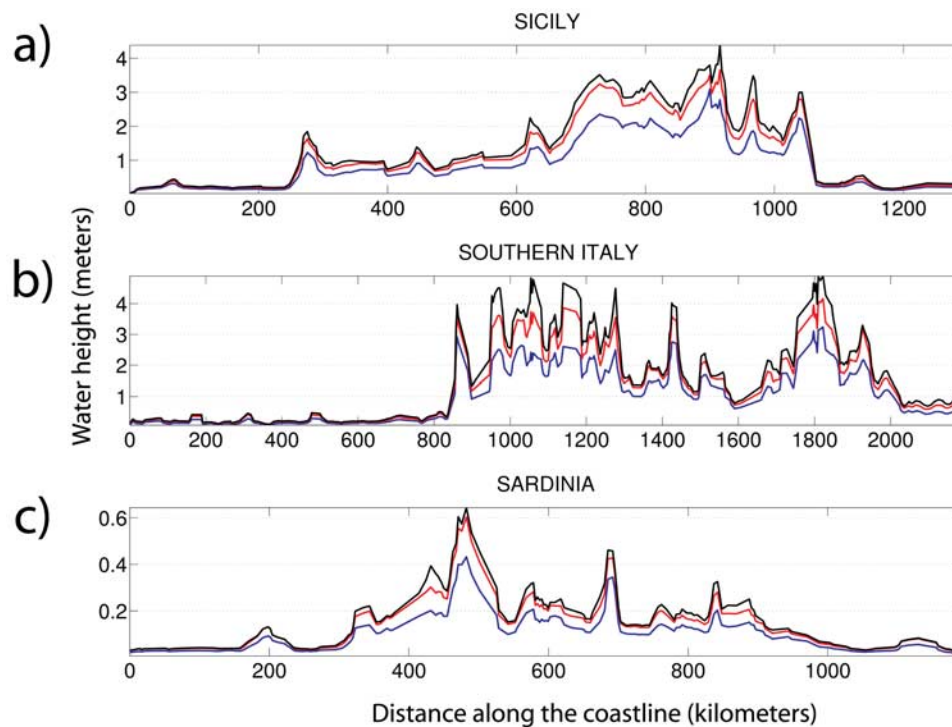


Figure 8. Hellenic Arc Source Zone. See Figure 6 for panel and symbol explanations.

branches orthogonal to fault strike. Predicted traveltimes of the wave crests for the TF (Figure 3c) show that the highest waves would reach the nearest Sardinia coastal locations in a few tens of minutes. Figure 3d also shows that the first wave would strike Cagliari only about 25–30 min after an earthquake has occurred on the sample TF. It will generally take a longer time (>30 min) for the first wave to reach any other location along both the coasts of Sicily and peninsular Southern Italy. Only the fault at the very western end of the SZ could generate a wave that reaches Sicily earlier than Sardinia (data not shown).

[38] Figure 6 shows the effects of the Algeria-Tunisia SZ, aggregated for all floating faults (15 in total, see Table 2). The strongest impact is seen on the coast of Sardinia, where the maximum wave height is frequently higher than 0.5 m, sometimes higher than 1.5 m, and is negligible only in the northwestern part of the island (between 1,000 and 1,200 km, Figure 2). Although the average wave heights rarely exceed 0.5 m, the standard deviations are quite large indicating that the effects on a given location may change significantly depending on the position of the source fault. Accordingly, the marigrams at Trapani, Napoli, Oristano and Cagliari (Figure 3d) appear in general more consistent with the average HMAXs than with their maxima. That is to say that the southernmost Sardinia coast, for example, would be more intensely hit by tsunamis generated by faults located in the easternmost part of the SZ (Figure 3a) than by those located in the western part.

[39] The maximum wave height generated by any fault belonging to this SZ on the coasts of Sicily and peninsular Southern Italy is generally less than half of that calculated for Sardinia. The maximum wave height is practically negligible in peninsular Southern Italy, apart from a short stretch including the southernmost part of the Gulf of

Salerno and the northern coasts of Cilento (350 to 400 km), and to a lesser extent the Gulf of Naples and the northernmost part of the Gulf of Salerno. Similarly, the Sicily coast is affected by a non-negligible maximum wave height (on the order of 0.5 m) only on its western side, from about Cinisi to Sciacca (between 100 and 450 km). The biggest potential threat is posed to the zone around Castellammare del Golfo (160 to 180 km) and between Trapani and Marsala (200 to 300 km).

4.2. Southern Tyrrhenian Source Zone

[40] The TF of this Source Zone (Figure 4a) produces very low energy tsunamis (Figure 4b). Significant waves on the northern Sicily coasts are predicted only in the case of north-dipping faults. Relatively high waves, however, may reach scattered localities on the western coast of peninsular Southern Italy. In case of occurrence of the MCE for the TF, predicted traveltimes of the wave crests (Figure 4c) indicate that the tsunami may take even less than 10 min to reach the nearest localities on the coast of northern Sicily. Palermo and its adjoining beaches will be reached by the first wave pulse in slightly more than 10 min (Figure 4d), but it will take much longer (>30 min) to reach the coasts peninsular of Southern Italy. A fault located at the very eastern end of the SZ, however, may generate a tsunami wave that reaches the coast of northeastern Sicily in less than 5 min and the Calabrian coasts in about 10 min.

[41] Figure 7 shows the aggregated results for all the floating faults (53 in total, see Table 2) of the Southern Tyrrhenian SZ. In general, predicted tsunami waves, even their maxima (black lines), do not exceed 0.2 m, as confirmed by the marigrams corresponding to the TF earthquake at Napoli, Vibo Valentia and Orosei (Figure 4d). Significantly higher waves (>0.5 m) affect only few local-

ities, scattered on the coast of northern Sicily (Figure 7a), such as Palermo itself and Trapani (in the distance range 0–300 km), and particularly around Milazzo and the coast west of it (1,100–1,300 km). This further indicates that faults of this SZ produce only local effects, as suggested also by the strong difference between the marigrams at Palermo and Messina (Figure 4d).

4.3. Hellenic Arc Source Zone

[42] The TF of this Source Zone (Figure 5a) focuses its energy along the SW-NE direction (Figure 5b). Waves higher than 1 m (more than 5 m at some places) are predicted along the coasts of northern Africa, mainly in Libya, in the Aegean islands and along the coasts all around the source. Probably as a result of edge waves, significant energy is trapped and carried along the coast of Egypt. Waves are amplified by strong shoaling effects along their propagation path toward the eastern coast of Tunisia. Similarly, local extreme HMAX values are observed at Malta and along the southeastern coasts of Sicily, Calabria and Apulia. The traveltime map (Figure 5c) shows that it takes about 60–70 min for the first wave to reach Southern Italy. Waves up to about 2 m reach Siracusa and Catanzaro (Figure 5d) 70 min after the earthquake. It is worth noticing, however, that the same tsunami reaches the nearest locations on the coast of Libya in about 30 min with waves higher than 1 m.

[43] Figure 8 shows the aggregated effects of all floating faults of this SZ (9 in total, see Table 2). Waves with average HMAX (blue line) of 1 m or higher are predicted to impact the coasts of most of southern and eastern Sicily (Figure 8a, between 280 and 1,050 km, from Trapani to Siracusa and Messina) and the southeastern coasts of peninsular Southern Italy (Figure 8b, between 850 and 2,000 km, from Reggio Calabria to Catanzaro, Taranto, Brindisi and almost to Bari). At Taranto, located at about 1,540 km along the Southern Italy coastline, a peak wave of more than 1 m would be observed in case of activation of the TF of this SZ (Figure 5d). Still higher peak waves would strike Siracusa and Catanzaro (Figure 5d). The average values are often higher than 2 m (Figure 8) and are sometimes not very different from the maximum values. Extreme values exceeding 4 m are very common all along the southeastern coast of peninsular Southern Italy. The Adriatic coast of Apulia beyond 2,000 km (Figure 8b) shows comparatively low wave heights (see also the marigram at Bari in Figure 5d) of less than 1 m. However, coastlines affected by generally low waves may experience occasional peaks as in the case of the westernmost corner of Sicily (Figure 8a, at about 250 km). In contrast, Sardinia seems to be rather well shielded by the landmass of Tunisia and Sicily for it experiences waves of less than 0.5 m that generally take more than 4 h to reach its coasts (data not shown). Only the area of the Cagliari Gulf may experience higher waves (Figure 8c, at about 480 km).

4.4. Comparison of the Three SZs

[44] Our predictions show that in terms of tsunami wave heights, the Algeria-Tunisia and Southern Tyrrhenian SZs affect the coast of Sicily in a similar way. Somewhat higher waves are expected only along the northern Sicily coasts, but they peak at over 0.5 m in a few places only. Conversely,

traveltimes to Sicily from the Algeria-Tunisia SZ are much longer than those from the Southern Tyrrhenian SZ (in the case of the TF, 40–50 vs. 10 min respectively). These results depict very different scenarios to be carefully considered in the implementation of tsunami (early) warning procedures.

[45] In contrast, the Hellenic Arc SZ may affect heavily all east-facing coasts of Sicily and Calabria. Predicted tsunami waves are generally higher than 1 m, peaking at over 3 m at several locations, and arrival times range between 50 and over 90 min depending on the exact source location. The same SZ is predicted to be able to hit the Ionian and Adriatic coasts of Apulia with tsunami waves up to 5 m high traveling in 60–100 min.

[46] The coasts of peninsular Southern Italy facing the Tyrrhenian Sea are well shielded from tsunamis generated in the Hellenic Arc. Conversely, they are exposed to tsunamis generated in the Algeria-Tunisia SZ, with traveltimes of half an hour or more, whereas the effects expected from the Southern Tyrrhenian SZ are negligible.

[47] Expected tsunami effects of the Hellenic Arc SZ on the coasts of Sardinia are stronger than those of the Southern Tyrrhenian SZ, but these effects would take place hours after the source event. This is remarkable considering the large difference in distance and that only waves propagating from the Hellenic Arc all the way through the Sicily Channel may reach Sardinia. However, Sardinia is expected to be hit more strongly and after a shorter time (in less than 30 min in the worst case) by waves generated by the Algeria-Tunisia SZ.

5. Discussion and Conclusions

[48] We investigated the potential effect on the Southern Italy Italian coasts of three Mediterranean Sea earthquake source zones that are known to be capable of generating large tsunamis: the Southern Tyrrhenian thrust, located at short distance from the Italian coasts; the Tell system, located at intermediate distance in the western Mediterranean; and the Hellenic trench, located at longer distance in the eastern Mediterranean. We calculated 77 tsunami scenarios based on a novel approach that combines a rather detailed knowledge of the tectonic setting of the source zones with the evaluation of the tsunami impact onto the target coastlines expected for each zone. Similarly to the work done in Japan [Yamazaki *et al.*, 2006] or New Zealand [Berryman, 2005], we stress that determining the characteristics of the potential earthquakes sources beforehand through geologic and tectonic studies yields substantially more realistic scenarios than can be easily compared with historically observed tsunamis.

[49] For each source zone we determined a Maximum Credible Earthquake (MCE) on the basis of observed earthquakes and a Typical Fault (TF) capable of generating it. TFs do not pretend to represent in detail all local situations, but are intended to represent an average geometry for the finite-fault input in the tsunami simulation. In the future, the determination of the MCE and of the TF could benefit from estimations obtained from finite element geodynamic models. Such models can predict realistic and reliable source lengths and earthquake magnitudes in regions where macroseismic or instrumental earthquake information is limited or

absent. This is the case of the Southern Tyrrhenian SZ, for which *Jenny et al.* [2006] and *Billi et al.* [2007] predicted a maximum magnitude ≥ 7.0 , substantially larger than that used in this work and observed historically.

[50] The Italian peninsula and Sicily are exposed to tsunamis generated both in the western and in the eastern Mediterranean. Our results show that the Sicily Channel and the Messina Straits separate the Mediterranean basin into two sub-basins and effectively act as barriers for E-W tsunami propagation. This conclusion had already been reached by *Tinti et al.* [2005] for a single scenario of a large tsunami offshore Eastern Sicily, but the large amount of scenarios we calculated in this work allows us to generalize it to all major Mediterranean source zones. One can conclude that, as a first order approximation, many countries whose coastlines face only one of the two sub-basins will not be affected by tsunamis generated in the other sub-basin. However, only a systematic identification of all possible sources along with their correlative tsunami scenarios will definitely help addressing this issue. The reader may refer to the Website http://diss.rm.ingv.it/medtsunami/S2_D1.4.html, that contains a series of elaborations performed within the project that supported our research.

[51] Our analysis also suggests that, given the relatively small size of the Mediterranean basin compared to the Pacific or Indian oceans, the identification of all possible sources of earthquake-generated tsunamis is indeed feasible, and that our method can be extended and replicated for different target coastlines (e.g., southern and eastern Spain, southern France, Greece, north Africa). A similar transnational effort would set the foundations of a comprehensive scenario database for the whole Mediterranean basin to help natural-disaster mitigation planners in devising appropriate countermeasures and develop preparedness strategies. This database would also form the basis for near-real-time threat assessment in case of a large earthquake; given its preliminary location and magnitude, it would be possible to quickly retrieve the tsunami simulation from the database instead of starting it from scratch.

[52] The method we propose is also suitable to serve as a basis for probabilistic tsunami hazard analyses such as that proposed by *Geist and Parsons* [2006]. A complete assessment of tsunami hazard, however, would involve the production of inundation maps of selected coastal sections, for example densely populated coastal areas and/or areas around the main harbors. Any further step, however, requires the creation of a publicly available bathymetry-topography database for coastal zones at the scale of at least a few hundred meters. In this case, the influence of local bathymetry on the accuracy of the calculated coastal wave heights could be better assessed.

[53] Finally, our work emphasizes the need for considering distant in addition to local sources, as we have shown that the occurrence of the MCE in the Hellenic Arc may represent a much more significant threat than many local sources. Recall that the MCE in the Hellenic Arc will impact the Southern Italy coasts with up to 5 m-high waves, comparable to those generated by the 28 December 1908 Messina earthquake (M_w 7.2), the source of the largest XX century Mediterranean tsunami, but will affect a much larger region. Similar circumstances (large far-field sources turning out to be a bigger threat than nearby but smaller

sources) could apply to most other Mediterranean coastlines. In other words, the assessment and subsequent mitigation of tsunami risk in the Mediterranean must necessarily be conducted at the scale of the entire basin and hence must involve a truly transnational effort.

[54] **Acknowledgments.** This work was funded by the project "Assessing the seismogenic potential and the probability of strong earthquakes in Italy" funded by the Italian Civil Defense through INGV-DPC Project S2, grants to RB and AP. MMT was supported by the project "Development of new technologies for the protection of the Italian territory from natural hazards" funded by the Italian Ministry of University and Research. SL was supported by the Italian Civil Defense. Thoughtful reviews from S. Ward and an Anonymous significantly improved the manuscript.

References

- Alasset, P.-J., H. Hébert, S. Maouche, V. Calbini, and M. Meghraoui (2006), The tsunami induced by the 2003 Zemmouri earthquake ($M_w = 6.9$, Algeria): Modelling and results, *Geophys. J. Int.*, *166*, 213–226, doi:10.1111/j.1365-246X.2006.02912.x.
- Benetatos, C., A. Kiratzi, C. Papazachos, and G. Karakaisis (2004), Focal mechanisms of shallow and intermediate depth earthquakes along the Hellenic Arc, *J. Geodyn.*, *37*, 253–296, doi:10.1016/j.jog.2004.02.002.
- Berryman, K. (Ed.) (2005), Review of Tsunami Hazard and Risk in New Zealand, *Client report 2005/104*, 139 pp., Institute of Geological & Nuclear Sciences.
- Bezzeghoud, M., D. Dimitrov, J. C. Ruegg, and K. Lammali (1995), Faulting mechanism of the El Asnam (Algeria) 1954 and 1980 earthquakes from modelling of vertical movements, *Tectonophysics*, *249*, 249–266.
- Billi, A., D. Presti, C. Faccenna, G. Neri, and B. Orecchio (2007), Seismotectonics of the Nubia plate compressive margin in the south Tyrrhenian region, Italy: Clues for subduction inception, *J. Geophys. Res.*, *112*, B08302, doi:10.1029/2006JB004837.
- Bohnhoff, M., J. Makris, D. Papanikolaou, and G. Stavrakakis (2001), Crustal investigation of the Hellenic subduction zone using wide aperture seismic data, *Tectonophysics*, *343*, 239–262.
- Bohnhoff, M., H.-P. Harjes, and T. Meier (2005), Deformation and stress regimes in the Hellenic subduction zone from focal mechanisms, *J. Seismol.*, *9*, 341–366, doi:10.1007/s10950-005-8720-5.
- Boschi, E., E. Guidoboni, G. Ferrari, D. Mariotti, G. Valensise, and P. Gasperini (eds.) (2000), Catalogue of strong Italian earthquakes from 461 B.C. to 1997, *Ann. Geofis.*, *43*, with CD-Rom, 259 pp.
- Casten, U., and K. Snopek (2006), Gravity modelling of the Hellenic subduction zone - a regional study, *Tectonophysics*, *417*, 183–200, doi:10.1016/j.tecto.2005.11.002.
- D'Agostino, N., and G. Selvaggi (2004), Crustal motion along the Eurasia-Nubia plate boundary in the Calabrian Arc and Sicily and active extension in the Messina Straits from GPS measurements, *J. Geophys. Res.*, *109*(B11), B11402, doi:10.1029/2004JB002998.
- Delouis, B., and M. Vallée (2003), The 2003 Boumerdes (Algeria) earthquake: Source process from teleseismic data, *CSEM Lett.*, *20*, 8–9, <http://www.emsc-csem.org>.
- Delouis, B., M. Vallée, M. Meghraoui, E. Calais, S. Maouche, K. Lammali, A. Mahsas, P. Briole, F. Benhamouda, and K. Yelles (2004), Slip distribution of the 2003 Boumerdes-Zemmouri earthquake, Algeria, from teleseismic, GPS, and coastal uplift data, *Geophys. Res. Lett.*, *31*, L18607, doi:10.1029/2004GL020687.
- Déverchère, J., K. Yelles, and E. Calais (2003), Active deformation along the Algerian Margin (MARADJA cruise): Framework of the May 21, 2003, M_w 6.8 Boumerdes earthquake, *Eos Trans. AGU*, *84*(46), Fall Meet. Suppl., Abstract S42E-0216.
- Déverchère, J., et al. (2005), Active thrust faulting offshore Boumerdes, Algeria, and its relations to the 2003 M_w 6.9 earthquake, *Geophys. Res. Lett.*, *32*, L04311, doi:10.1029/2004GL021646.
- Domzig, A., et al. (2006), Searching for the Africa-Eurasia Miocene boundary offshore western Algeria (MARADJA'03 cruise), *C. R. Geoscience*, *338*, 80–91, doi:10.1016/j.crte.2005.11.009.
- Earthquake Engineering Research Institute (2003), The Boumerdes, Algeria, Earthquake of May 21, 2003, *EERI Learning from Earthquakes Reconnaissance Report*, EERI, Oakland, California.
- El-Sayed, A., F. Romanelli, and G. F. Panza (2000), Recent seismicity and realistic waveforms modeling to reduce the ambiguities about the 1303 seismic activity in Egypt, *Tectonophysics*, *328*, 341–357.
- Faccenna, C., L. Jolivet, C. Piromallo, and A. Morelli (2003), Subduction and the depth of convection in the Mediterranean mantle, *J. Geophys. Res.*, *108*(B2), 2099, doi:10.1029/2002JB001690.

- Faccenna, C., C. Piromallo, A. Crespo-Blanc, L. Jolivet, and F. Rossetti (2004), Lateral slab deformation and the origin of the western Mediterranean arcs, *Tectonics*, 23, TC1012, doi:10.1029/2002TC001488.
- Flemming, N. C. (1978), Holocene eustatic changes and coastal tectonics in the Northeastern Mediterranean: implications for models of crustal consumption, *Philos. Trans. R. Soc. London Ser. A, Mathematical and Physical Sciences*, 289(1362), 405–458.
- Geist, E. L., and T. Parsons (2006), Probabilistic analysis of tsunami hazards, *Natural Hazards*, 37, 277–314, doi:10.1007/s11069-005-4646-z.
- Goes, S., D. Giardini, S. Jenny, C. Hollenstein, H.-G. Kahle, and A. Geiger (2004), A recent tectonic reorganization in the South-Central Mediterranean, *Earth Planet. Sci. Lett.*, 225, 335–345, doi:10.1016/j.epsl.2004.07.038.
- Gruppo di lavoro CPTI (2004), Catalogo Parametrico dei Terremoti Italiani, versione 2004 (CPTI04). INGV, Bologna (also available at: <http://emidius.mi.ingv.it/CPTI04/>).
- Guidoboni, E., A. Comastri, and G. Traina (1994), *Catalogue of ancient earthquakes in the Mediterranean area up to the 10th century*, 504 pp., I.N.G. and S.G.A., Bologna, Italy.
- Gutscher, M.-A., J. Roger, M.-A. Baptista, J. M. Miranda, and S. Tinti (2006), Source of the 1693 Catania earthquake and tsunami (southern Italy): New evidence from tsunami modeling of a locked subduction fault plane, *Geophys. Res. Lett.*, 33, L03809, doi:10.1029/2005GL025442.
- Hamouda, A. Z. (2006), Numerical computations of 1303 tsunamigenic propagation towards Alexandria, Egyptian Coast, *J. African Earth Sci.*, 44(1), 37–44.
- International Seismological Centre (2001), On-line Bulletin, <http://www.isc.ac.uk/Bull/>, Internat. Seismol. Cent., Thatcham, United Kingdom.
- Jenny, S., S. Goes, D. Giardini, and H.-G. Kahle (2006), Seismic potential of Southern Italy, *Tectonophysics*, 415, 81–101, doi:10.1016/j.tecto.2005.12.003.
- Kahle, H.-G., M. Cocard, Y. Peter, A. Geiger, R. Reilinger, A. Barka, and G. Veis (2000), GPS-derived strain rate field within the boundary zones of the Eurasian, African and Arabian Plates, *J. Geophys. Res.*, 105(B10), 23,353–23,370, doi:10.1029/2000JB900238.
- Kanamori, H., and E. E. Brodsky (2004), The physics of earthquakes, *Rep. Prog. Phys.*, 67(8), 1429–1496.
- Løvholt, F., H. Bungum, C. B. Harbitz, S. Glimsdal, C. D. Lindholm, and G. Pedersen (2006), Earthquake related tsunami hazard along the western coast of Thailand, *Nat. Hazards Earth Syst. Sci.*, 6, 979–997.
- Mader, C. L. (2001), *Numerical modeling of water waves*, Los Alamos series in Basic and Applied Sciences, 206 p.
- Makris, J., and T. Yegorova (2006), A 3-D density-velocity model between the Cretan Sea and Libya, *Tectonophysics*, 417, 201–220, doi:10.1016/j.tecto.2005.11.003.
- McClusky, S., et al. (2000), Global Positioning System constraints on plate kinematics and dynamics in the eastern Mediterranean and Caucasus, *J. Geophys. Res.*, 105(B3), 5695–5719, doi:10.1029/1999JB900351.
- Meghraoui, M., and F. Doumaz (1996), Earthquake-induced flooding and paleoseismicity of the El Asnam, Algeria, fault-related fold, *J. Geophys. Res.*, 101(B8), 17,617–17,644, doi:10.1029/96JB006050.
- Meghraoui, M., S. Maouche, B. Chema, Z. Cakir, A. Aoudia, A. Harbi, P.-J. Alasset, A. Ajadi, Y. Bouhadad, and F. Benhamouda (2004), Coastal uplift and thrust faulting associated with the $M_w = 6.8$ Zemmouri (Algeria) earthquake of 21 May, 2003, *Geophys. Res. Lett.*, 31, L19605, doi:10.1029/2004GL020466.
- Nocquet, J.-M., and E. Calais (2004), Geodetic measurements of crustal deformation in the Western Mediterranean and Europe, *Pure Appl. Geophys.*, 161, 661–681, doi:10.1007/s00024-003-2468-z.
- Okada, Y. (1985), Surface deformation due to shear and tensile faults in a half-space, *Bull. Seismol. Soc. Am.*, 75, 1135–1154.
- Okada, Y. (1992), Internal deformation due to shear and tensile faults in a half-space, *Bull. Seismol. Soc. Am.*, 82, 1018–1040.
- Papazachos, C., and G. Nolet (1997), P and S deep velocity structure of the Hellenic area obtained by robust nonlinear inversion of travel times, *J. Geophys. Res.*, 102(B4), 8349–8367.
- Papazachos, B., and C. Papazachou (1997), *The earthquakes of Greece*, 304 pp., Editions Ziti, Thessaloniki, Greece.
- Papazachos, B., V. G. Karakostas, C. B. Papazachos, and E. M. Scordiliis (2000), The geometry of the Wadati-Benioff zone and lithospheric kinematics in the Hellenic arc, *Tectonophysics*, 319, 275–300.
- Pareschi, M. T., E. Boschi, F. Mazzarini, and M. Favalli (2006a), Large submarine landslides offshore Mt. Etna, *Geophys. Res. Lett.*, 33, L13302, doi:10.1029/2006GL026064.
- Pareschi, M. T., M. Favalli, and E. Boschi (2006b), Impact of the Minoan tsunami of Santorini: Simulated scenarios in the eastern Mediterranean, *Geophys. Res. Lett.*, 33, L18607, doi:10.1029/2006GL027205.
- Pelinovsky, E., C. Kharif, I. Riabov, and M. Francius (2002), Modelling of tsunami propagation in the vicinity of the French coast of the Mediterranean, *Natural Hazards*, 25(2), 135–159, doi:10.1023/A:1013721313222.
- Pepe, F., A. Sulli, G. Bertotti, and R. Catalano (2005), Structural highs formation and their relationship to sedimentary basins in the north Sicily continental margin (southern Tyrrhenian Sea): Implication for the Drepano Thrust Front, *Tectonophysics*, 409, 1–18, doi:10.1016/j.tecto.2005.05.009.
- Philip, H., and M. Meghraoui (1983), Structural analysis and interpretation of the surface deformations of the El Asnam earthquake of October 10, 1980, *Tectonics*, 2, 17–49.
- Piatanesi, A., and S. Tinti (1998), A revision of the 1693 eastern Sicily earthquake and tsunami, *J. Geophys. Res.*, 103(B2), 2749–2758.
- Piatanesi, A., and S. Tinti (2002), Numerical modeling of the September 8, 1905 Calabrian (southern Italy) tsunami, *Geophys. J. Int.*, 150, 271–284.
- Pirazzoli, P. A., J. Thommeret, Y. Thommeret, J. Laborel, and L. F. Montaggioni (1982), Crustal block movements from Holocene shorelines: Crete and Antikythira (Greece), *Tectonophysics*, 86, 27–43.
- Pirazzoli, P. A., J. Laborel, and S. C. Stiros (1996), Earthquake clustering in the Eastern Mediterranean during historical times, *J. Geophys. Res.*, 101(B3), 6083–6097.
- Piromallo, C., and A. Morelli (2003), P-wave tomography of the mantle under the Alpine-Mediterranean area, *J. Geophys. Res.*, 108(B2), 2065, doi:10.1029/2002JB001757.
- Pondrelli, S., C. Piromallo, and E. Serpelloni (2004), Convergence vs. retreat in southern Tyrrhenian Sea: Insights from kinematics, *Geophys. Res. Lett.*, 31, L06611, doi:10.1029/2003GL019223.
- Power, W., G. Downes, and M. Stirling (2007), Estimation of tsunami hazard in New Zealand due to south American earthquakes, *Pure Appl. Geophys.*, 164, 547–564, doi:10.1007/s00024-006-0166-3.
- Ruegg, J. C., K. Kasser, A. Tarantola, J. C. Lepine, and B. Chouikrat (1982), Deformations associated with the El Asnam earthquake of 10 October 1980: Geodetic determination of vertical and horizontal movements, *Bull. Seismol. Soc. Am.*, 72, 2227–2244.
- Satake, K., K. Shimazaki, Y. Tsuji, and U. Kazue (1996), Time and size of a giant earthquake in Cascadia inferred from Japanese tsunami records of January 1700, *Nature*, 379, 246–249.
- Semmane, F., M. Campillo, and F. Cotton (2005), Fault location and source process of the Boumerdes, Algeria, earthquake inferred from geodetic and strong motion data, *Geophys. Res. Lett.*, 32, L01305, doi:10.1029/2004GL021268.
- Serpelloni, E., M. Anzidei, P. Baldi, G. Casula, and A. Galvani (2005), Crustal velocity and strain-rate fields in Italy and surrounding regions: New results from the analysis of permanent and non-permanent GPS networks, *Geophys. J. Int.*, 161, 861–880, doi:10.1111/j.1365-246X.2005.02618.x.
- Serpelloni, E., G. Vannucci, S. Pondrelli, A. Argnani, G. Casula, M. Anzidei, P. Baldi, and P. Gasperini (2007), Kinematics of the Western Africa-Eurasia plate boundary from focal mechanisms and GPS data, *Geophys. J. Int.*, 169, 1180–1200, doi:10.1111/j.1365-246X.2007.03367.x.
- Smith, W. H. F., and D. T. Sandwell (1997), Global sea floor topography from satellite altimetry and ship depth soundings, *Science*, 277, 1956–1962.
- Soloviev, S. L. (1990), Tsunamigenic zones in the Mediterranean Sea, *Natural Hazards*, 3, 183–202, doi:10.1007/BF00140432.
- Stiros, S. C., and A. Drakos (2006), A fault-model for the tsunami-associated, magnitude ≥ 8.5 Eastern Mediterranean, AD 365 earthquake, *Z. Geomorph. N. F., Suppl.-Vol. 146*, 125–137.
- Tinti, S., and A. Piatanesi (1996), Numerical simulations of the tsunami induced by the 1627 earthquake affecting Gargano, Southern Italy, *J. Geodynamics*, 21, 141–160.
- Tinti, S., A. Maramai, and L. Graziani (2001), A new version of the European tsunami catalogue: Updating and revision, *Nat. Haz. Earth Syst. Sci.*, 1, 255–262.
- Tinti, S., A. Maramai, and L. Graziani (2004), The new catalogue of Italian tsunamis, *Natural Hazards*, 33(3), 439–465.
- Tinti, S., A. Armigliato, G. Pagnoni, and F. Zaniboni (2005), Scenarios of giant tsunamis of tectonic origin in the Mediterranean, *ISET J. Earthquake Technology, Paper n. 464*, 42(4), 171–188.
- Tinti, S., G. Pagnoni, and F. Zaniboni (2006), The landslides and tsunamis of the 30th of December 2002 in Stromboli analysed through numerical simulations, *Bull. Volcanol.*, 68(5), 462–479.
- Titov, V. V., F. I. González, E. N. Bernard, M. C. Eble, H. O. Mofjeld, J. C. Newman, and A. J. Venturato (2005), Real-time tsunami forecasting: Challenges and solutions, *Natural Hazards*, 35(1), Special Issue, U.S. National Tsunami Hazard Mitigation Program, 41–58, doi:10.1007/s11069-004-2403-3.
- Yamazaki, Y., Y. Wei, K. F. Cheung, and G. D. Curtis (2006), Forecast of tsunami from the Japan-Kuril-Kamchatka source region, *Natural Hazards*, 38, 411–435, doi:10.1007/s11069-005-2075-7.
- Yelles, K., K. Lammali, and A. Mahsas (2004), Coseismic deformation of the May 21st, 2003, $M_w = 6.8$ Boumerdes earthquake, Algeria, from GPS measurements, *Geophys. Res. Lett.*, 31, L13610, doi:10.1029/2004GL019884.
- Valensise, G., and D. Pantosti (Eds.) (2001), Database of potential sources for earthquakes larger than $M 5.5$ in Italy, *Ann. Geofis., Suppl. to vol. 44(4)*, 797–964, with CD-ROM.

- Vannucci, G., and P. Gasperini (2004), The new release of the database of earthquake mechanisms of the Mediterranean area (EMMA Version 2), *Ann. Geophys.*, Suppl. to vol. 47(1), 307–334.
- Vannucci, G., S. Pondrelli, A. Argani, A. Morelli, P. Gasperini, and E. Boschi (2004), An atlas of Mediterranean seismicity, *Ann. Geophys.*, Suppl. to vol. 47(1), 247–306.
- Wells, D. L., and K. J. Coppersmith (1994), New empirical relationships among magnitude, rupture length, rupture width, rupture area, and surface displacement, *Bull. Seismol. Soc. Am.*, 84, 974–1002.
- Wortel, M. J. R., and W. Spakman (2000), Subduction and slab detachment in the Mediterranean-Carpathian region, *Science*, 290, 1910–1917, doi:10.1126/science.290.5498.1910.
-
- R. Basili, S. Lorito, A. Piatanesi, M. M. Tiberti, and G. Valensise, Istituto Nazionale di Geofisica e Vulcanologia, Sezione di Sismologia e Tettonofisica, Via di Vigna Murata 605, 00143 Rome, Italy. (roberto.basili@ingv.it; lorito@ingv.it; piatanesi@ingv.it; tiberti@ingv.it; valensise@ingv.it)